Molecules on vicinal Au surfaces studied by scanning tunnelling microscopy

2006 J. Phys.: Condens. Matter 18 S51

(http://iopscience.iop.org/0953-8984/18/13/S04)

INSTITUTE OF PHYSICS PUBLISHING JOURNAL OF PHYSICS: CONDENSED MATTER

J. Phys.: Condens. Matter **18** (2006) S51–S66 doi:10.1088/0953-8984/18/13/S04

Molecules on vicinal Au surfaces studied by scanning tunnelling microscopy

J Kröger[1], N Néel[1], H Jensen[1], R Berndt[1], R Rurali[2] and N Lorente[2]

[1] Institut für Experimentelle und Angewandte Physik, Christian-Albrechts-Universität zu Kiel, D-24098 Kiel, Germany
[2] Laboratoire Collisions, Agrégats, Réactivité, Université Paul Sabatier, F-31062 Toulouse, France

E-mail: kroeger@physik.uni-kiel.de

Received 30 September 2005
Published 13 March 2006
Online at stacks.iop.org/JPhysCM/18/S51

Abstract

Using low-temperature scanning tunnelling microscopy and spectroscopy we investigated the adsorption characteristics of 3,4,9,10-perylenetetracarboxylic-dianhydride and fullerenes on Au(788), Au(433), and Au(778). On Au(788) and Au(778), 3,4,9,10-perylenetetracarboxylic-dianhydride exhibits three coexisting superstructures, which do not reflect the periodicity of the hosting substrate. The adsorption on Au(433) leads to the formation of molecule chains along the step edges after annealing the sample. Fullerene molecules on Au(788) arrange in a mesh of islands, which extends over several hundreds of nanometres with an extraordinarily high periodicity. A combination of fullerene adsorption and annealing leads to facetting of Au(433) and the formation of extraordinarily long fullerene stripes.

(Some figures in this article are in colour only in the electronic version)

1. Introduction

The central issue of this work is self-organization, which is a promising approach for fabricating structures on the nanometre scale. In fact, the last decade has witnessed many efforts to realize the parallel fabrication of long-range ordered nanostructures on surfaces. The controlled fabrication of highly periodic metal [1], semiconductor [2, 3], or molecular [4] nanostructures at surfaces remains, however, a challenging endeavour in nanoscience research. Large quantities of structures can be created in parallel by self-organized growth, either in the kinetic [5] or the thermodynamic regime [2, 3, 6] and the controlled deposition of size-selected clusters from the gas phase [7]. Owing to the statistical nature of deposition and diffusion processes it is difficult to achieve lateral order by this approach. Consequently, prestructured samples have been studied intensely to enhance ordering on a large scale. On planar surfaces, for

instance, the use of strained layers and dislocations as templates for subsequent deposition led to a self-organization on the scale of several dozens of nanometres [1, 5]. Supramolecular surface assemblies can be guided using hydrogen bonding [8, 9] to control and guide new surface phases formed by subsequently deposited molecules [4]. A highly regular mesh of hexagonal boron nitride was recently fabricated by self-organization on a Rh(111) single-crystalline surface [10] and led to ordering of C_{60} molecules. An alternative approach is to use vicinal surfaces, i.e., surfaces which correspond to small deviations from the most symmetric crystallographic planes. They represent periodic arrays of steps at the nanometre scale with adjustable dimensions and thus are of great interest for the fabrication of nanowires [11–13] or quantum dots [14, 15]. However, as we will show in this article, vicinal surfaces do not automatically serve as templates for regular and periodic adsorption patterns. The design of such patterns requires the adequate combination of adsorbate and substrate. As a further approach to achieve large-scale periodic structures we mention here the use of surface stress. Surface stress is expected to play a crucial role in fabricating devices with highly uniform and predictable electrical, magnetic, or optical properties [16–20]. However, it is difficult to establish the link between stress and morphology in experiments because key kinetic or thermodynamic parameters necessary for a quantitative interpretation are often not known. As a consequence, the fabrication of nanostructures exploiting surface stress is a challenging task. One promising way to achieve nanoscale patterning is the use of adsorbates which induce facetting of surfaces. The thermodynamic stability of vicinal surfaces is governed by the free energy of the respective low-index facet, the step creation energy, and the free energy of step–step interaction. Any change of thermodynamic variables such as temperature or the chemical potential of an adsorbate which alters the relative contributions of these energetic terms may result in orientational instability of a vicinal surface. As a consequence facetting, i.e., the breakup of the surface into facets with different orientation, can occur [21]. This phenomenon has been known for a long time [22] and was demonstrated in experiments on surfaces vicinal to Si(111) [23] and on surfaces vicinal to GaAs(100) [24, 25]. These systems revealed facetting upon annealing of a cleaved surface or upon growth interruption. On metallic surfaces, oxygen on vicinal Ag(110) [26], and oxygen [27] and potassium [28] on vicinal of Cu(100) lead to a facetting of the surfaces. Facetting is not limited to adsorbed atoms and has also been observed, for example, after deposition of molecules on metallic surfaces [29, 30]. The resulting facetted morphology enables the fabrication of organized arrays with distinct physical and chemical properties on the same surface.

In this work we review our recent research on the adsorption characteristics of 3,4,9,10-perylenetetracarboxylic-dianhydride (PTCDA) and C_{60} on vicinal gold surfaces. Interest in organic molecular films is fuelled by technological advances in organic devices [31, 32], potential applications in molecular switches [33, 34], and functionalization of surfaces [35–37] as well as by the fundamental understanding of the film–metal system [38–40]. Typically, the geometric and electronic structure of the molecule–substrate interface is of substantial importance. Therefore considerable effort has been made to investigate this interface and to maximize its homogeneity [41]. Owing to the complexity of molecular shapes and interactions, however, perfectly homogeneous interfaces usually remain elusive, and coexistence of structural domains has been reported for various molecular systems [42]. Detailed characterization of the variability of the electronic structure on a single molecule scale requires high lateral resolution and has, consequently, hardly been achieved [43, 44]. The C_{60} molecule has attracted considerable attention owing to its remarkable stability and to its applications as an acceptor unit in photovoltaic devices and as a unique platform for supramolecular chemistry [45, 46]. Ordered layers of C_{60} can be used as templates for additional deposition due to their higher corrugation than atomic surfaces [47]. Polymerization

of C_{60} layers on surfaces is of considerable interest concerning the use of fullerenes as material-resistive masks for high-resolution photolithography [48].

The article is organized as follows. In section 2 we introduce briefly the vicinal surfaces employed in our studies. As a first system we present the adsorbate PTCDA on Au(788), Au(778), and Au(433) (section 3). As a main result we obtain that vicinal surfaces do not always act as templates for subsequent deposition. For Au(788)–PTCDA and Au(778)–PTCDA we observe a coexistence of PTCDA adsorption phases, which do not reflect the periodicity of the hosting substrate surfaces. Interestingly, the different adsorption phases reveal distinct electronic properties. As we show by single-molecule tunnelling spectroscopy, the energy of molecular orbitals depends upon the superstructure the molecules are embedded in. For Au(433)–PTCDA we arrive at molecule chains along the step edges after annealing the sample surface. In section 4 we show that by a suitable choice of the molecule and the vicinal surface the template properties of the vicinal surface can be exploited. We report on an easy-to-prepare self-organized array of fullerene islands on a stepped gold surface. Self-organized two-dimensional C_{60} islands occur on Au(788) and form a well ordered rectangular array extending over distances of hundreds of nanometres and covering almost the entire crystal surface. The high quality of this periodic structure together with its easy fabrication render this adsorption system a promising candidate for directing further deposition of functional units. The submonolayer deposition of C_{60} on Au(433) is analysed in section 5. As a main result we show that facetting of the substrate surface is induced by a combination of C_{60} adsorption and subsequent annealing. The resulting surface exhibits an alternation of adjacent fullerene and substrate stripes revealing lengths of several hundreds of nanometres.

2. The clean vicinal surfaces: Au(788), Au(778), Au(433)

In this section we briefly introduce the vicinal gold surfaces, which were used in our experiments. Figure 1 shows constant-current STM images of Au(788) (figure 1(a)), Au(433) (figure 1(b)), and Au(778) (figure 1(c)). The use of vicinal Au(788) was motivated by its *a priori* two-dimensional periodic patterning [14]. This surface consists of a periodic succession of {111} minifacets separated by 3.9 nm wide (111) terraces. The terraces are reconstructed with the discommensuration lines perpendicular to the step edges, separating face-centred cubic (fcc) and hexagonal close-packed (hcp) stacking fault domains with a periodicity of 7.2 nm (see inset of figure 1(a)). Step edges and discommensuration lines together represent a regular periodic pattern all over the sample (figure 1(a)). The Au(433) vicinal surface is comprised of a periodic succession of (111) terraces and {100} steps [49]. (111) terraces of 4.0 nm width are separated by a set of (on average) six terraces each 1.4 nm wide. The preferential adsorption of C_{60} at step edges on various metal samples at submonolayer coverage [50, 51] together with the strong interaction of fullerenes with Au(111) [52] renders Au(433)–C_{60} a promising candidate for realizing ordered arrays of C_{60} stripes and gold terraces. Vicinal Au(778) consists of (111) terraces delimited by {100} steps. The width of the terraces is 3.6 nm.

3. PTCDA on Au(111) vicinals

A model system of electronic studies of an organic–inorganic interface at the molecular level is PTCDA. The adsorption geometry of PTCDA on metal surfaces was analysed previously as excellently reviewed by Witte and Wöll [42] and Barlow and Raval [53]. Adsorption characteristics on Au(111) deserve special interest since this surface exhibits a $22 \times \sqrt{3}$ reconstruction. Chizhov *et al* [54] found that room-temperature adsorption leads to two

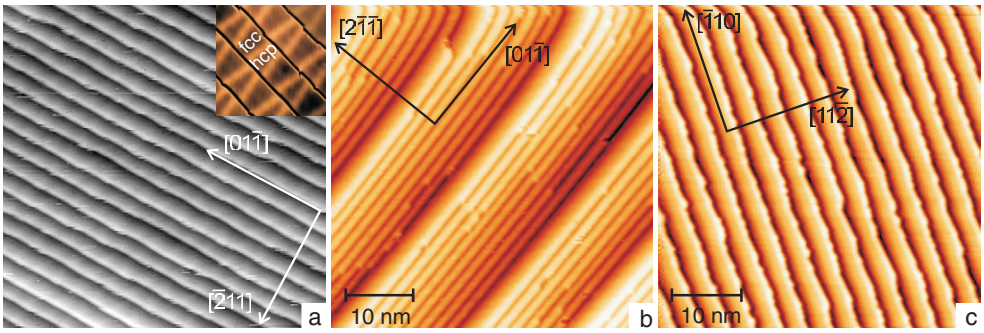

Figure 1. Constant-current STM images of (a) Au(788), the direction of ascending steps runs from the bottom left of the image to its top right (inset: close-up view with enhanced contrast to highlight the discommensuration lines running perpendicularly to the step edges), (b) Au(433), and (c) Au(778).

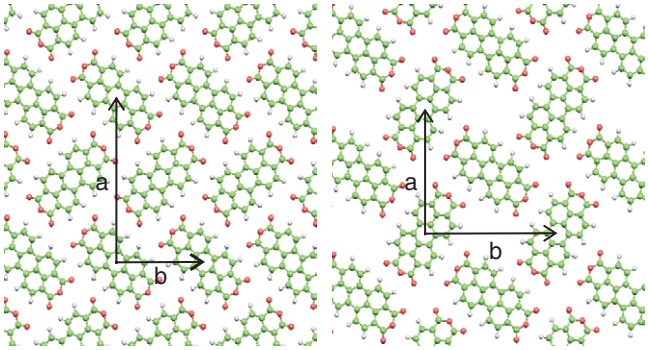

Figure 2. Left panel: PTCDA herringbone structure with indicated unit cell vectors. Right panel: PTCDA square phase with indicated unit cell vectors.

coexisting adsorbate geometries, namely a herringbone structure and a square phase. Bulk PTCDA reveals the herringbone structure in (102) crystalline planes (see figure 2, left panel), whereas the square phase consists of PTCDA molecules adsorbed on the boundary of a square with equivalent axes of adjacent molecules including an angle of 90° (figure 2, right panel). In a recent STM study of Au(788)–PTCDA [55] with molecules deposited onto the surface held at room temperature we showed that another square phase coexists with the herringbone and square adsorption structure introduced in figure 2. In this domain PTCDA molecules likewise adsorb on the boundary of a square, but in contrast to the previous square phase ends of molecules point to the centres of adjacent molecules. In the following we will focus on the structures presented in figure 2. Figure 3 shows constant-current STM images of 0.25 ML PTCDA on Au(788). From a large-scale image, where PTCDA islands appear as bright contrast, it is already clear that the PTCDA molecules do not arrange according to the periodicity of the vicinal surface. Figure 3(b) shows a close-up view of the image presented in figure 3(a). We can distinguish the three PTCDA adsorption superstructures introduced above: the herringbone domain (denoted as A), the square phase which is also observed on Au(111) [54] (denoted as B), and the second square phase (denoted as C), which occurs less frequently than A and B on this surface. The dimensions of the unit cell vectors in domain A are $a = (1.12 \pm 0.07)$ nm and $b = (1.79 \pm 0.09)$ nm; in domain B we find

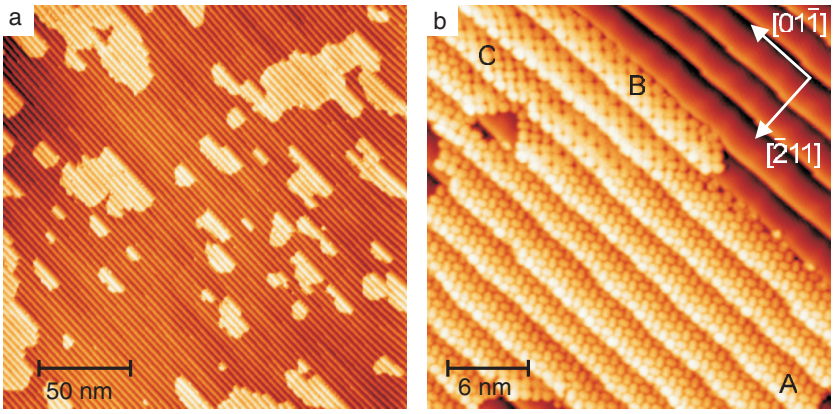

Figure 3. (a) Overview constant-current STM image of Au(788) covered with 0.25 ML PTCDA (tunnelling parameters: $V = 1000$ mV, $I = 100$ pA; size: 220 nm × 220 nm). (b) Close-up view of a scan area in (a) revealing three adsorption domains denoted as A, B, and C. Crystal directions are indicated. ($V = 1000$ mV, $I = 100$ pA, 33 nm × 33 nm.)

$a = b = (1.44 \pm 0.12)$ nm. As an important result we notice from these observations that Au(788) does not act as a template to guide PTCDA adsorption. Rather than this, intermolecular interactions seem to govern the adsorption superstructures since the PTCDA molecules do not adhere to the periodicity provided by the vicinal surface. The PTCDA superstructures on Au(788) exhibit intriguing electronic properties as exemplified by the A and B adsorption phase. Figure 4 presents constant-current STM images recorded at the indicated tunnelling voltages. The images show four PTCDA-covered Au(788) terraces where A and B domains are visible in the lower and upper part, respectively. At 400 mV all PTCDA molecules are imaged as structureless rectangles. For 800 mV topographic changes of the A phase are hardly visible while intramolecular structure emerges in the B phase, the former rectangular shape of the molecules being lost in favour of a hexagonal shape. Finally, at 1200 mV submolecular structure is observed for both domains. These observations strikingly demonstrate that the electronic structure underlying the intramolecular contrast depends on the adsorption phase of PTCDA molecules. We notice that occasionally in the B phase entities are coordinated by four adjacent PTCDA molecules. These entities are assigned to single trapped substrate atoms.

To interpret these data we performed calculations within density functional theory (DFT) with the code SIESTA [56] using a double-ζ basis set plus polarization functions [57] for the valence electrons and the generalized gradients approximation (GGA) [58] for the exchange–correlation functional. The Au(111) surface serves as a model of the terraces of Au(788). Various supercell sizes in a slab geometry were explored to take into account different packing densities of PTCDA superstructures. For simulating experimental spectra of the differential conductivity we calculated the local density of states at the tip apex, being 0.7 nm above the surface. Due to the weak molecule–surface interaction local and semi-local approaches of DFT fail to yield the correct adsorption parameters of PTCDA on Au(111). Here, we are interested in a qualitative analysis of the electronic structure. A recent incidence x-ray standing wave experiment performed on Ag(111)–PTCDA determined the vertical distance of the perylene core to be ≈0.28 nm [59]. Hence, we have frozen the height of the molecular atoms at 0.28 nm and allowed a full relaxation of the other molecular coordinates in order to find the correct packing geometry for the two molecules constituting our supercell. Our calculations show that increasing the adsorption height by 0.1 nm leads to a basically free molecule, which

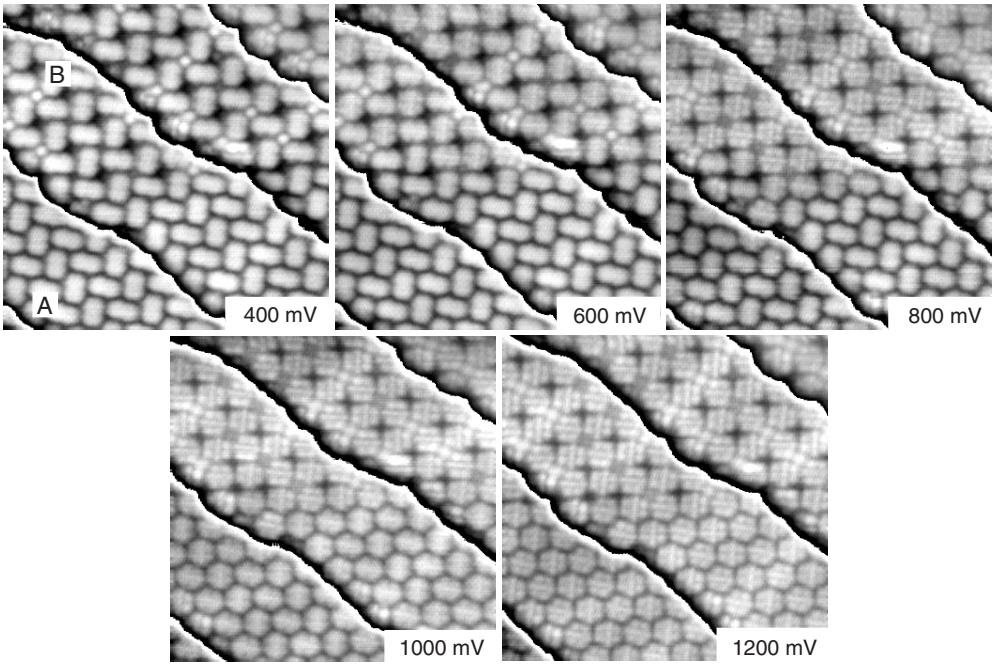

Figure 4. Sequence of constant-current images recorded at characteristic sample voltages. The top (bottom) part of each image shows B-domain (A-domain) molecules ($I = 200$ pA, 12 nm × 12 nm). A periodic greyscale is used to highlight the contrasts on each terrace.

slightly interacts with the surface. Decreasing the molecule–surface distance by 0.03 nm leads to a very large mixing of molecular orbitals because the molecule is already probing the strongly repulsive substrate potential. With this theoretical background we first trace the origin of the submolecular contrast back to the involved molecular orbitals. Figure 5(a) shows the differential conductivity $\mathrm{d}I/\mathrm{d}V$ as acquired in the centre of a single PTCDA molecule embedded in the herringbone adsorption domain. We find a single peak centred at ≈1.1 eV. The calculated $\mathrm{d}I/\mathrm{d}V$ spectrum, shown as a full line, matches the experimental spectrum. In the calculation, the main contribution to the conductivity originates from the density of states of the second-to-lowest unoccupied molecular orbital (LUMO + 1). The LUMO + 2 is basically degenerate with the LUMO + 1 and also contributes to the spectroscopic signature giving a certain broadening of the peak. Since the intramolecular structure for herringbone-phase molecules appears above ≈1 V we ascribe most of the submolecular structure to the spatial distribution of the LUMO + 1. In both phases the submolecular contrast looks very similar, which leads us to attribute the submolecular contrast of the square phase likewise to the spatial distribution of the LUMO + 1 density of states. As a consequence the energetic position of the LUMO + 1 depends on the local environment of the individual molecule and thus differs for molecules embedded in different domains. We further tested this hypothesis by single-molecule spectroscopy of the differential conductivity acquired above the centre of B-phase and A-phase molecules (figure 5(b), open and solid circles, respectively). The spectral signature of B-phase PTCDA is located at ≈0.8 eV, i.e., shifted by ≈0.35eV compared to the A phase. Owing to the similar intramolecular contrast in both phases we can safely attribute this peak to the LUMO + 1. Since the feedback loop was frozen at 850 mV the LUMO + 1 contribution of the A-phase molecule has not yet developed leading to a smaller tip–molecule

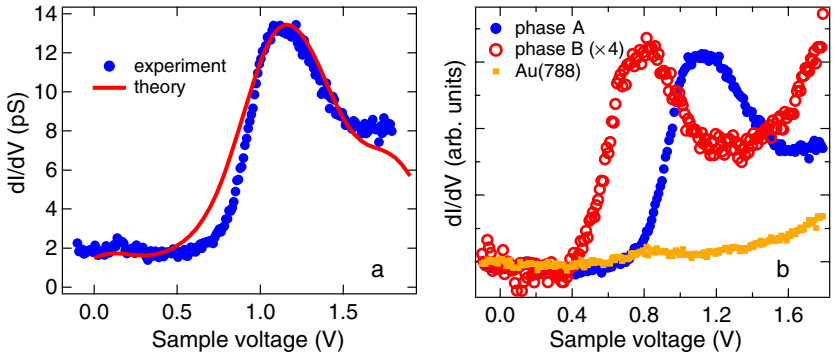

Figure 5. (a) Experimental (solid circles) and calculated (full line, fitted to the experimental maximum; the peak includes a numerical broadening of 0.25 eV) $\mathrm{d}I/\mathrm{d}V$ spectra of a single PTCDA molecule in the herringbone adsorption domain (A). Feedback loop parameters: $V = 1.4$ V, $I = 200$ pA. (b) Spectra of $\mathrm{d}I/\mathrm{d}V$ versus sample voltage on bare Au(788) (dots), on B-domain PTCDA (open circles), and on A-domain PTCDA (solid circles). Maxima of $\mathrm{d}I/\mathrm{d}V$ occur at $\approx$0.8 V and $\approx$1.1 V for B- and A-domain PTCDA, respectively. The feedback loop was frozen at $V = 850$ mV, $I = 200$ pA. Data for B-domain PTCDA were multiplied by 4.

distance than in the case of the B-phase molecule. To show both peaks on the same scale we multiplied the data acquired on the B-phase molecule by a factor of 4. Spectra of occupied electronic states, i.e., at negative voltages ($-2.5\ \mathrm{V} \leqslant V \leqslant 0$), turned out to be featureless. Our calculations predict, for instance, the LUMO of PTCDA to be pinned at the Fermi level [59]. The spatial distribution of the LUMO density of states is found to adhere strongly to the molecule and to be less evanescent into vacuum than the LUMO + 1. This leads to its efficient suppression from the $\mathrm{d}I/\mathrm{d}V$ spectra (as observed in our experiments).

At present, an explanation for the experimentally observed molecular orbital energy shift is not available. Below we discuss a variety of scenarios, which may lead to the different binding energies. The shift might be due to (i) the specific choice of Au(788), (ii) different work functions in the different adsorption phases, (iii) different adsorption heights, (iv) influence of the tip's electric field, (v) an adsorbate-induced modification of the metallic surface, (vi) the entities surrounded by four PTCDA molecules in the B phase, or, (vii), a hydrogen-bond-induced molecule–molecule interaction. The first scenario can be excluded since we observe the same energy shift on Au(778), where likewise A- and B-type adsorption phases exist. On Au(111), the molecular orbitals in question appear at the same energies as observed for Au(788) [55] and consequently we can infer that the vicinal character of the surfaces does not play an important role for the energy shift. The ability of DFT to reproduce workfunction changes even in the case of physisorbed molecules [60] led us to compute the workfunction changes and compare with experimental data. Within experimental accuracy the workfunction change between adsorption domains A and B is at most 0.1 eV, which agrees well with the change of the two molecular phases frozen at 0.28 nm from the surface atomic plane. The implications of this result are twofold. First, the workfunction change is not able to explain the energy shift of 0.35 eV and, second, the molecules lie at the same molecule–surface distance in both phases. Different combinations of molecular heights for the two phases led to inconsistent results and to disagreement with the measured workfunction change. As a consequence, scenarios (ii) and (iii) can be safely excluded as well. The electric field of the tip has been included in the calculation by computing the electronic structure for different values of external electrical fields as large as 2 eV nm^{-1} without a sizeable effect on the $\mathrm{d}I/\mathrm{d}V$ peak

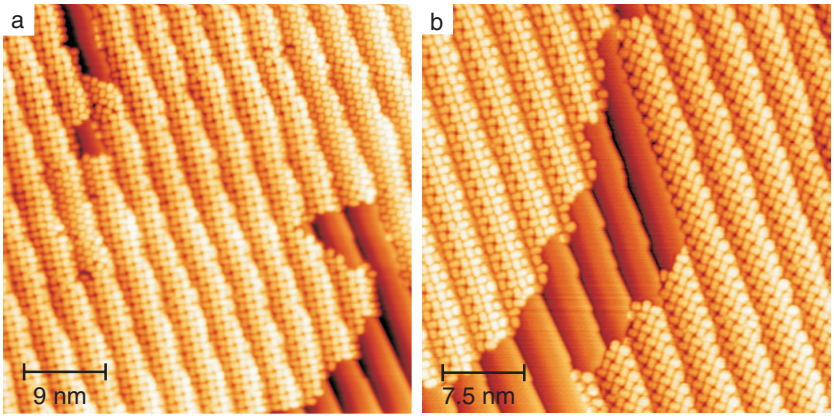

Figure 6. (a) Low-temperature constant-current STM image of Au(778)–PTCDA after deposition at room temperature and without annealing. The random distribution of herringbone and square adsorption domains on the terraces is obvious ($V = 500$ mV, $I = 500$ pA, 45 nm $\times$ 45 nm). (b) Constant-current STM image of Ag(778)–PTCDA at 9 K. The sample was annealed at 480 K prior to imaging ($V = 450$ mV, $I = 220$ pA, 38 nm $\times$ 38 nm).

position. The model electric field was homogeneous and perpendicular to the surface. The modification of the metallic surface is unlikely due to the very weak physisorption interaction. The single substrate atoms, which are trapped in the centre of four B-phase molecules, can be safely ruled out from driving the orbital shift for the following reasons. First, from figure 4 we can infer that all molecules of the B phase simultaneously reveal the submolecular contrast. This observation points to a negligible effect of the trapped atom on the molecular electronic structure. In fact, single-molecule tunnelling spectroscopy on all B-phase molecules exhibits the same orbital shift with respect to A-phase molecules. Second, on Au(111)–PTCDA we likewise observe A and B adsorption phases revealing the same molecular orbital shift. However, we have never encountered single atoms trapped by B-phase molecules. Finally, we address scenario (vii), where hydrogen-bond-induced molecule–molecule interactions are supposed to drive the orbital energy shift. Hydrogen bonds were shown to play an important role for the interaction between various molecules on various substrates [61–63]. Our calculations indicate that apart from the molecule–substrate interaction the intermolecular one plays a role. The latter is mediated by hydrogen bonding between adjacent molecules. Additionally, the molecule adsorption geometry, which cannot be accurately described within DFT [64], may also play a role for the orbital energy shift. As discussed in more detail in [55], we infer that the packing density and the actual adsorption geometry can influence the energetic positions of molecular orbitals.

We close this section by comparing the adsorbate systems Au(778)–PTCDA and Au(433)–PTCDA. Corresponding constant-current STM images are presented in figures 6 and 7 for Au(778) and Au(433), respectively. Deposition of PTCDA molecules on Au(778) in the submonolayer range at room temperature leads to constant-current STM images as shown in figure 6(a). We observe the coexistence of a herringbone and a square PTCDA superstructure as already known from PTCDA adsorption on Au(788) (see figure 3(b)). These superstructures persist when the sample is annealed at $\approx$480 K after deposition (figure 6(b)). The adsorption behaviour of PTCDA on Au(433) is shown in figure 7. Figure 7(a) presents a constant-current STM image of Au(433)–PTCDA after depositing the molecules at room temperature and cooling to 9 K. The wide terraces are embraced by molecule chains: on one side of the wide

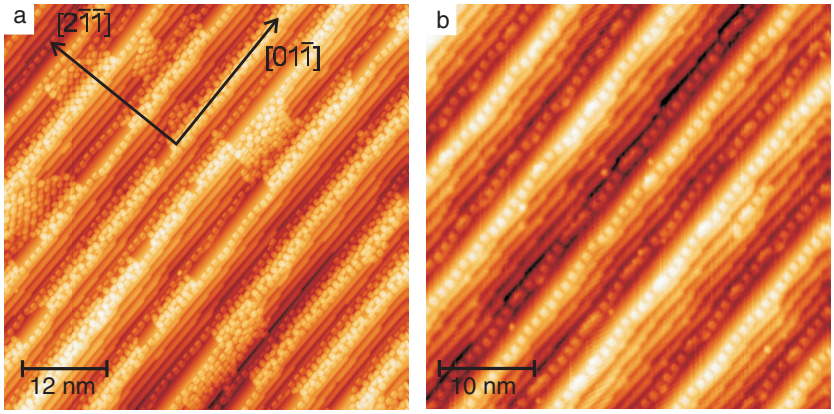

Figure 7. (a) Constant-current STM image of Au(433)–PTCDA at 9 K. Step edges, step bunches and wide terraces are occupied with PTCDA without long-range order ($V = -100$ mV, $I = 220$ pA, 30 nm $\times$ 30 nm). (b) Constant-current STM image of Au(433)–PTCDA after annealing the covered surface at 480 K. Preferential adsorption at the step edges is observed ($V = 300$ mV, $I = 270$ pA, 45 nm $\times$ 45 nm).

terrace PTCDA molecules adsorb with their lower end on the wide terrace and with their upper end on the adjacent narrow terrace; on the opposite side the upper end of PTCDA is adsorbed on the wide terrace whilst its lower end adsorbs on the adjacent narrow terrace. The long axis of the molecule (see figure 2) is oriented perpendicular to the step edge direction. Additionally we find small islands of PTCDA on the wide terraces, which exhibit locally the herringbone and the square superstructure. Also the step bunches of Au(433) are covered by molecules, where likewise no long-range ordering of superstructures is observed. After annealing an equivalently prepared sample, constant-current STM images at 9 K look like the one depicted in figure 7(b). Only the molecule chains embracing the wide terraces remained.

As a result, we are faced with two different adsorption scenarios on vicinal gold surfaces whose terrace orientation and minifacet type are the same. An explanation for this effect is not available at present. At very low PTCDA coverages on Au(778) the molecules form chains at step edges, which are similar to those observed on Au(433). With increasing coverage, however, these chains are substituted by islands on the Au(778) terraces. Consequently, while both the adsorption of molecular chains and two-dimensional islands are possible on these surfaces, the molecules show a strong preference for one of these structures depending on coverage and local substrate geometry. Possibly the formation of PTCDA islands as observed on Au(788) and on Au(778) is feasible only because of molecule diffusion across the step edges. Since on Au(433) the step bunches do not belong to preferential adsorption sites (molecules adsorbed at step bunches do not persist annealing; see figure 7(b)), the diffusion across the step bunches may be hindered. This results in the adsorption of molecular chains along the step edges being the more favourable adsorption behaviour on the (433) surface.

4. C_{60} on Au(788)

We chose Au(788) again as the supporting substrate because of its *a priori* two-dimensional patterning [14]. Further, room-temperature deposition of C_{60} at very low coverage on Au(111) was shown to lead to an adsorption only on step fcc segments [50, 65]. A reason for the preferential adsorption site has not yet been given. Initial growth of 1-nitronaphtalene on

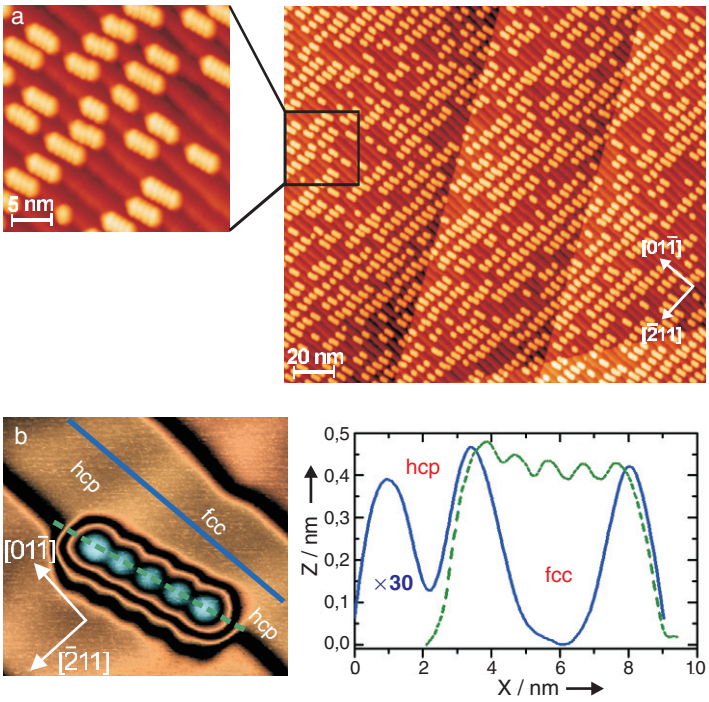

Figure 8. (a) Constant-current STM images of Au(788)-C_{60} at low coverage. The direction of ascending steps runs from the bottom left to the top right of the images ($V = 750$ mV, $I = 100$ pA). (b) Left panel: constant-current STM image of Au(788)-C_{60} at low coverage (-1500 mV, 0.5 nA, 8 nm × 9 nm) showing a chain of five C_{60} adsorbed on the upper part of the step edge. The corrugation due to the terrace levels has been subtracted in order to enhance the details both on the fullerene chain and on the terraces. Right panel: line profiles taken from the STM image shown in the left panel across the plain terrace (full line) and across the molecule chain (dashed line). Line scan data of Au(788) were multiplied by 30 to obtain a common height scale.

Au(111) likewise occurs exclusively on the fcc domain of the surface reconstruction [8]. In this case total energy calculations with different top-layer stackings were performed to find the effect of the Au(111) surface reconstruction on the 1-nitronaphtalene physisorption [63]. As a result the selectivity of the molecule adsorption was traced back to a combination of a less stable adsorption at step hcp sites than at step fcc sites and a weak adsorption at the boundaries between fcc and hcp regions. We propose a similar scenario to hold for Au(788)-C_{60}. An alternative scenario, which may explain this adsorption behaviour, is related to a possible interaction of fullerene molecules with the Au(788) electronic surface state. As was shown by Chen *et al* [66], the $22 \times \sqrt{3}$ reconstruction of Au(111) (which separates fcc from hcp stacking domains like on Au(788)) imposes a periodic potential for the surface state electrons. As a consequence the local density of states at the surface state binding energy is lower on the fcc than in the hcp domains. On the other hand, from surface-state-mediated adsorbate–adsorbate interactions it is known that the mutual distance between adsorbates is such as to occupy local minima of the Friedel-type local-density-of-states oscillations [67, 68]. Consequently, PTCDA analogously may prefer adsorption sites with low surface-state density of states, which is provided by the fcc stacking domains of Au(788). As a consequence, the Au(788) surface seemed to serve as a promising template for realizing an ordered array of fullerene nanostructures [69]. Regular meshes of Co islands on Au(788) with lateral extensions of the order of 100 nm were reported

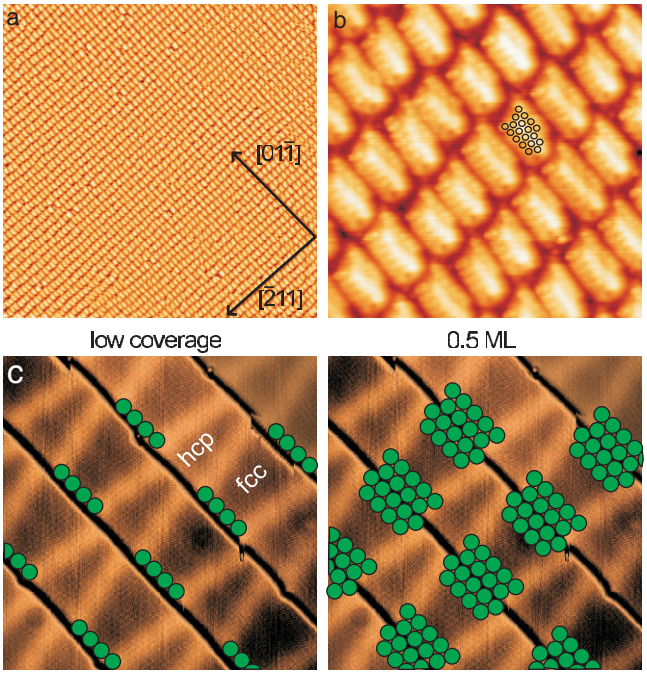

Figure 9. (a) Constant-current STM image of 0.5 ML C_{60} on Au(788) (750 mV, 100 pA, 280 nm × 280 nm). Ascending step direction bottom left to top right. (b) Close-up view of STM image in (a) (32 nm × 32 nm) revealing molecularly resolved (black circles) fullerene islands. (c) Proposed adsorption geometry. The full circles represent fullerene molecules. Left panel: low coverage; right panel: nanomesh coverage of 0.5 ML.

previously [14]. In figure 8(a) we show a low-temperature (9 K) constant-current STM image of Au(788)–C_{60} at low coverage (adsorption of fullerene molecules was performed at room temperature). The direction of ascending steps runs from the bottom left to the top right of the image. As can be seen from the close-up view in figure 8(a) (left panel) the fullerene chains adsorb on the upper part of the step edges. We focus on a single C_{60} chain in the left panel of figure 8(b), where we enhanced the contrast of the constant-current STM image to see both the molecules and the discommensuration lines of the Au(788) surface. Obviously, the C_{60} molecules preferentially adsorb at the fcc stacking areas. To corroborate this hypothesis, we show in the right panel of figure 8(b) linescans of the uncovered Au(788) terrace (full line) and of the C_{60} chain (dashed line). The three peaks of the terrace profile are related to the discommensuration lines embracing the hcp and fcc regions as indicated in the left panel of figure 8(b). From the profiles it is evident that the fullerene chains nucleate exclusively on the fcc sites, as observed previously on Au(111) [50, 65]. We can thus explain the low-coverage constant-current STM image displayed in figure 8(a): the preferential adsorption site for fullerene molecules are the fcc stacking domains. As a consequence, alternating stripes of occupied fcc sites and adjacent stripes of unoccupied hcp sites develop perpendicular to the step edge direction. On Au(788), the longest molecule chains that can be hosted by the 4.2 nm wide fcc domains consist of five C_{60}, which have a length of 3.9 nm (measured between the molecule centres). Longer chains can appear where parts of the step edge locally deviate from the [01$\bar{1}$] direction, leading to an extended length of the fcc domain at the step edge. A constant-current STM image of Au(788) covered with 0.5 ML C_{60} is presented in

figure 9(a). Here self-organization of C_{60} islands of almost rectangular shape is observed. The longer sides of the islands are oriented along the substrate step edges. These islands are organized in an unusually well ordered two-dimensional rectangular array, which extends over several hundreds of nanometres. The high degree of periodicity and the low defect density are obvious. Statistically we find a period along $[01\bar{1}]$ of (7.2 ± 0.1) nm, while the period along $[\bar{2}11]$ is (4.0 ± 0.4) nm. The larger variation of the periodicity along $[\bar{2}11]$ is due to the intrinsic larger width of the terrace length distribution of the Au(788) surface [14]. The observed regular mesh of fullerene islands thus reflects the periodicity of the substrate surface. Judging from a large number of recorded images we estimate that this periodic array covers more than 90% of the total crystal surface. The presented STM image in figure 9 (a) is consequently representative of the nanostructuring of this surface after deposition of 0.5 ML of C_{60}. Only areas where orientations differed from the Au(788) plane, for example, areas with step bunches, misorientations of the crystal, large terraces, or kinked steps, showed a different morphology. As a consequence, the two-dimensional patterning of Au(788) acts as an ideal template for guiding fullerene adsorption. The structural perfection of the C_{60} layer is thus mainly controlled by the quality of the substrate. Given the high degree of substrate perfection that can be achieved (several micrometres without structural defects [70]) particularly well ordered molecular arrays can be fabricated. The close-up view in figure 9(b) illustrates the homogeneity of the fullerene island shape. Molecular resolution of the C_{60} (black circles indicate molecule positions) reveals that the molecules are arranged in a hexagonal lattice with one of the three main compact chain directions oriented along $[01\bar{1}]$. The observed nearest-neighbour distance of $\approx$1 nm is similar to the one found for the full monolayer coverage of C_{60} on Au(111) and Au(788). In the step descending direction, $[\bar{2}11]$, all islands have almost the same width corresponding to four compact chains of molecules. The distribution of chain lengths oriented along $[01\bar{1}]$ evaluated from 250 islands shows that most (94%) compact chains contain four to five C_{60} molecules. Only a few per cent contain three or six molecules, and no shorter or longer chains have been observed. In figure 9(c) on the basis of our low-coverage measurements (depicted in figure 8(a)) we propose a growth model. Initially (left panel of figure 9(c)) deposited C_{60} molecules diffuse on the flat terraces until they reach step edges where they adsorb and form chains occupying exclusively fcc segments (figure 8(c)). Once the step edge fcc segments are saturated by fullerene chains, additional C_{60} molecules nucleate at these chains from the lower and upper terrace, rather than filling the hcp segments. This process leads to the formation of islands as observed at a coverage of 0.5 ML (right panel of figure 9(c)).

In conclusion, we found that 0.5 ML C_{60} on Au(788) exhibits a highly periodic superstructure. The rectangular fullerene islands form an extraordinarily well ordered mesh extending over several hundreds of nanometres.

5. C_{60} on Au(433)

In this last section we present experimental results of submonolayer C_{60} deposition on the Au(433) surface [71]. We fabricated fullerene stripes by exploiting facetting of the surface, which we induced by annealing the Au(433) surface covered with 0.5 ML of C_{60}. The resulting surface exhibits an alternation of fullerene and substrate stripes, whose lengths are several hundreds of nanometres without interruption. Figure 10(a) shows a constant-current STM image of Au(433)–C_{60} where 0.5 ML of fullerene molecules were adsorbed at room temperature without subsequent annealing. Bright areas are covered by C_{60} molecules, which reside almost exclusively at the step bunches of Au(433). The wide terraces remain almost unoccupied. Along the step edge direction compact fullerene chains are observed with a mean

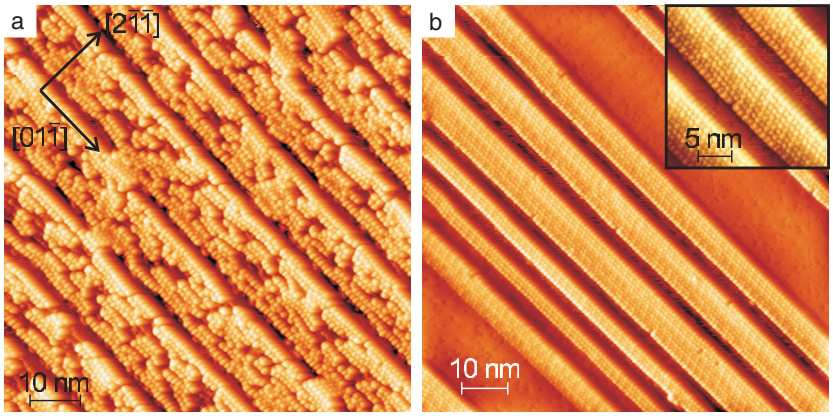

Figure 10. Constant-current STM images ($V = 1.5$ V, $I = 0.1$ nA, 88 nm $\times$ 88 nm) of 0.5 ML C_{60} on Au(433) deposited at room temperature: (a) without annealing and (b) after annealing at $T = 500$ K for 15 min (inset: close-up view of three adjacent fullerene stripes). The ascending step direction of the pristine vicinal surface runs from lower left corner to the upper right one.

distance between molecules of (1.0 ± 0.1) nm. Perpendicular to the step edge direction a wide distribution of distances between fullerene chains is observed. Only small areas of C_{60} layers where molecules are close packed in a hexagonal lattice are visible. Consequently, figure 10(a) displays a C_{60} adsorption layer, which is not homogeneous and does not reveal long-range hexagonal order. Increasing the coverage leads to an occupation of the wide terraces rather than completing unoccupied sites on the narrow terraces. As a consequence, increasing the amount of deposited molecules does not lead to homogeneous and close-packed fullerene stripes. In clear contrast, figure 10(b) shows a constant-current STM image of the same surface, which was annealed at 500 K for 15 min after deposition. Intriguingly, the morphology has changed and a facetting of the surface is clearly seen. The surface reveals two kinds of facets. Wide (111) gold terraces are separated by straight stripes of C_{60}, which exclusively adsorbed on the substrate step bunches. This self-organization results in an array of straight and parallel fullerene nanowires on the sample. Our observations show that the C_{60} stripes consist of compact fullerene chains and have an average width of six to eight such chains (see the inset of figure 11(a)). Figure 11(a) shows a series of three fullerene stripes of different widths. Line profiles taken across the step edge are averaged and presented in figure 11(b). The profile shows a line scan of a wide (111) terrace (line parallel to the x axis) and of C_{60} facets, which are inclined by an angle of $\alpha = (15 \pm 3)^\circ$ with respect to the (111) terrace. As a consequence, the faces of fullerene stripes with different widths exhibit the same orientation. The height difference between two (111) gold terraces delimiting a single fullerene stripe shows that the number of gold steps is equal to the number of C_{60} chains of the stripe. Consequently, the fullerene facets consist of C_{60} chains, which occupy a single terrace of the step bunch. Within the stripes the molecules are organized in a hexagonal lattice (see the inset of figure 11(a)) with a lattice parameter of (1.1 ± 0.1) nm. From this value the distance l_t between substrate steps can be extracted to give $l_t = (0.95 \pm 0.1)$ nm. Together with the facet inclination angle we infer a (533) orientation of the gold step bunches ($l_{t(533)} = 0.94$ nm, $\alpha_{(533)} = 14.4^\circ$). The facetting of vicinal surfaces after deposition of material is governed either by thermodynamics or by kinetics. In the latter case, the facetting is driven by the kinetic growth process and occurs during deposition. Since facetting of Au(433)–C_{60} is observed exclusively after annealing kinetic facetting can be ruled out for this adsorbate system. We propose the facetting to be caused by thermodynamics.

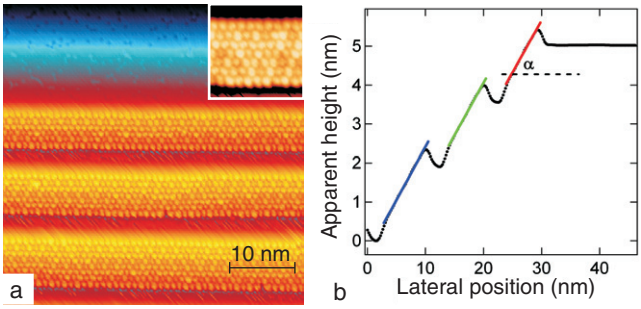

Figure 11. (a) Constant-current STM images ($V = 1.5$ V, $I = 0.1$ nA, 46 nm $\times$ 46 nm) of 0.5 ML covered Au(433)-C_{60} after annealing to 500 K. The fullerene stripes occur on the facetted Au(433) surface. The ascending step direction of the pristine vicinal surface runs from bottom to top of the image. Inset: close-up view of a C_{60} stripe. (b) Averaged line profile taken perpendicular to the step edge direction. The angle α describes the inclination of the fullerene stripes with respect to the (111) plane.

Thermodynamic facetting occurs in order to minimize the free energy of the surface. When molecules are adsorbed on a surface, intermolecular interactions are a component of the free energy. The room-temperature deposition of C_{60} without subsequent annealing revealed an inhomogeneous fullerene layer because of a mismatch between the terrace width and the mean distance between molecules. However, annealing of the surface enables the activation of a substrate interlayer mass transport process, which is necessary to decrease the terraces width within the step bunches. The observed fullerene layer configuration is thus energetically the most favourable one.

6. Summary

We reviewed our recent work on the adsorption characteristics of molecules on vicinal surfaces. The template function of vicinal surfaces to guide the adsorption is absent for PTCDA on Au(788) and Au(778), where we found different superstructures to coexist. Whilst these superstructures do not reflect the periodicity of the hosting substrate surface, they exhibit striking electronic properties. The energy of the PTCDA LUMO + 1 was shown to differ appreciably in the different superstructure. This effect was tentatively attributed to intermolecular interactions mediated by hydrogen bonds. The adsorption of C_{60} on Au(788) led to the formation of a highly regular mesh of fullerene islands with unprecedented periodicity and lateral extension. The mesh clearly reflects the periodicity of the Au(788) substrate. On Au(433), C_{60} adsorption induces a facetting of the substrate surface leading to a surface morphology which consists of an alternation of extremely long fullerene and substrate stripes.

Acknowledgments

We are delighted to thank M Sokolowski (University of Bonn, Germany), J E Ortega (Universidad del Pais Vasco, Spain), and C Cepek (Laboratorio Nazionale TASC, Synchrotron Trieste, Italy) for providing the PTCDA molecules, the Au(788) sample, and clean C_{60}. Fruitful discussions with B Hartke (University of Kiel, Germany) are gratefully acknowledged. We acknowledge financial support by the Deutsche Forschungsgemeinschaft through the ESF SONS program. RR acknowledges the financial support of the Generalitat de Catalunya through a NANOTEC fellowship.

References

[1] Chambliss D D, Wilson R J and Chiang S 1991 *Phys. Rev. Lett.* **66** 1721
[2] Nötzel R, Tommyo J and Tamamura T 1994 *Nature* **369** 131
[3] Moison J M, Houzay F, Barthe F, Leprince L, André E and Vatel D 1994 *Appl. Phys. Lett.* **64** 196
[4] Theobald J A, Oxtoby N S, Phillips M A, Champness N R and Beton P H 2003 *Nature* **424** 1029
[5] Brune H 1998 *Surf. Sci. Rep.* **31** 121
[6] Leonard D, Krishnamurthy M, Reaves C M, Denbaars S P and Petroff P M 1993 *Appl. Phys. Lett.* **63** 3203
[7] Roy H V, Fayet P, Patthey F, Schneider W D, Delley B and Massobrio C 1994 *Phys. Rev.* B **49** 5611
[8] Böhringer M, Morgenstern K, Schneider W D, Berndt R, Mauri F, De Vita A and Car R 1999 *Phys. Rev. Lett.* **83** 324
[9] Barth J V, Weckesser J, Cai C, Günter P, Bürgi L, Jeandupeux O and Kern K 2000 *Angew. Chem. Int. Edn Engl.* **39** 1230
[10] Corso M, Auwärter W, Muntwiler M, Tamai A, Greber T and Osterwalder J 2004 *Science* **303** 217
[11] Shen J, Skomski R, Klaua M, Jenniches H, Sundar Manoharan S and Kirschner J 1997 *Phys. Rev.* B **56** 2340
[12] Gambardella P, Blanc M, Brune H, Kuhnke K and Kern K 2000 *Phys. Rev.* B **61** 2254
[13] Lin J L, Petrovykh D Y, Kirakosian A, Rauscher H and Himpsel F J 2001 *Appl. Phys. Lett.* **78** 829
[14] Repain V, Baudot G, Ellmer H and Rousset S 2002 *Europhys. Lett.* **58** 730
[15] Ohno S, Yagyuu K, Nakatsuji K and Komori F 2002 *Japan. J. Appl. Phys.* **41** L1243
[16] Marchenko V I 1981 *JETP Lett.* **33** 382
[17] Alerhand O L, Vanderbilt D, Meade R D and Joannopoulos J D 1988 *Phys. Rev. Lett.* **61** 1973
[18] Vanderbilt D 1992 *Surf. Sci. Lett.* **268** L300
[19] Ng K O and Vanderbilt D 1995 *Phys. Rev.* B **52** 2177
[20] Seul M and Andelman D 1995 *Science* **267** 476
[21] Williams E D and Bartelt N C 1991 *Science* **251** 393
[22] Chernov A A 1984 *Modern Crystallography III* (Berlin: Springer)
[23] Williams E D, Phaneuf R J, Wei J, Bartelt N C and Einstein T L 1993 *Surf. Sci.* **294** 219
[24] Kasu M and Kobayashi N 1993 *Appl. Phys. Lett.* **62** 1262
[25] Golubok A O, Gur'yanov G M, Petrov V N, Samsonenko Y B, Tipisev S Y, Tsyrlin G E and Ledentsov N N 1994 *Semiconductors* **28** 317
[26] Ozcomert J S, Pai W W, Bartelt N C and Reutt-Robey J E 1994 *Phys. Rev. Lett.* **72** 258
[27] Chen Q and Richardson N V 2003 *Prog. Surf. Sci.* **73** 59
[28] Schwenger L and Ernst H J 1996 *Surf. Sci.* **347** 25
[29] Böhringer M, Berndt R and Schneider W D 1997 *Phys. Rev.* B **55** 1384
[30] Pascual J I, Barth J V, Ceballos G, Trimarchi G, De Vita A, Kern K and Rust H P 2004 *J. Chem. Phys.* **120** 11367
[31] Dimitrakopoulos C D, Purushothaman S, Kymissis J, Callegari A and Shaw J M 1999 *Science* **283** 822
[32] van Oijen A M, Ketelaars M, Köhler J, Aartsma T J and Schmidt J 1999 *Science* **285** 400
[33] Chen J, Reed M A, Rawlett A M and Tour J M 1999 *Science* **286** 1550
[34] Lahann J, Mitragotri S, Tran T N, Kaido H, Sundaram J, Choi I S, Hoffer S, Somorjai G and Langer R 2003 *Science* **299** 371
[35] Tang C W and VanSlyke S A 1987 *Appl. Phys. Lett.* **51** 913
[36] Burrows P E and Forrest S R 1993 *Appl. Phys. Lett.* **62** 3102
[37] Taylor R B, Burrows P E and Forrest S R 1997 *IEEE Photon. Technol. Lett.* **9** 365
[38] Böhringer M, Schneider W D, Berndt R, Glöckler K, Sokolowski M and Umbach E 1998 *Phys. Rev.* B **57** 4081
[39] Glöckler K, Seidel C, Soukopp A, Sokolowski M, Umbach E, Böhringer M, Berndt R and Schneider W D 1998 *Surf. Sci.* **405** 1
[40] Eremtchenko M, Bauer D, Schaefer J A and Tautz F S 2004 *New J. Phys.* **6** 4
[41] Forrest S R 1997 *Chem. Rev.* **97** 1793
[42] Witte G and Wöll Ch 2004 *J. Mater. Res.* **19** 1889
[43] Ludwig C, Gompf B, Petersen J, Strohmaier R and Eisenmenger W 1994 *Z. Phys.* B **93** 365
[44] Toerker M, Fritz T, Proehl H, Sellam F and Leo K 2001 *Surf. Sci.* **491** 255
[45] Hirsch A 1994 *Chemistry of the Fullerenes* (New York: Thieme)
[46] Shi B R, Wang X S, Huang H, Yang S H, Bachmann A and Cue N 2002 *J. Vac. Sci. Technol.* B **20** 2388
[47] Klyachko D and Chen D M 1997 *J. Vac. Sci. Technol.* B **15** 1295
[48] Hebard A F, Eom C B, Fleming R M, Chabal Y J, Muller A J, Glarum S H, Pietsch G J, Haddon R C, Mujsce A M, Paczkowski M A and Kochanski G P 1993 *Appl. Phys.* A **57** 299
[49] Rousset S, Repain V, Baudot G, Garreau Y and Lecoeur J 2003 *J. Phys.: Condens. Matter* **15** S3363
[50] Altman E I and Colton R J 1992 *Surf. Sci.* **279** 49
Altman E I and Colton R J 1992 *Surf. Sci.* **295** 13

[51] Motai K, Hashizume T, Shinoara H, Saito Y, Pickering H W, Nishina Y and Sakurai T 1993 *Japan. J. Appl. Phys.* **32** L450
[52] Altman E I and Colton R J 1993 *Phys. Rev.* B **48** 18244
[53] Barlow S M and Raval R 2003 *Surf. Sci. Rep.* **50** 201
[54] Chizhov I, Kahn A and Scoles G 2000 *J. Cryst. Growth* **208** 449
[55] Kröger J, Jensen H, Berndt R, Rurali R and Lorente N 2005 *Phys. Rev. Lett.* submitted
[56] Soler J, Artacho E, Gale J D, García A, Junquera J, Ordejón P and Sánchez-Portal D 2002 *J. Phys.: Condens. Matter* **14** 2745
[57] Anglada E, Soler J M, Junquera J and Artacho E 2002 *Phys. Rev.* B **66** 205101
[58] Perdew J P, Burke K and Ernzerhof M 1996 *Phys. Rev. Lett.* **77** 3865
[59] Hauschild A, Karki K, Cowie B C C, Rohlfing M, Tautz F S and Sokolowski M 2005 *Phys. Rev. Lett.* **94** 036106
[60] Morikawa Y, Ishi H and Seki K 2004 *Phys. Rev.* B **69** 041403
[61] Böhringer M, Morgenstern K, Schneider W D, Wühn M, Wöll Ch and Berndt R 2000 *Surf. Sci.* **444** 199
[62] Böhringer M, Schneider W D and Berndt R 2000 *Angew. Chem. Int. Edn* **39** 792
[63] Vladimirova M, Stengel M, DeVita A, Baldereschi A, Böhringer M, Morgenstern K, Berndt R and Schneider W D 2001 *Europhys. Lett.* **56** 254
[64] Rurali R, Lorente N and Ordejon P 2005 *Phys. Rev. Lett.* **95** 209601
[65] Fujita D, Yakabe T, Nejoh H, Sato T and Iwatsuki M 1996 *Surf. Sci.* **366** 93
[66] Chen W, Madhavan V, Jamneala T and Crommie M F 1998 *Phys. Rev. Lett.* **80** 1469
[67] Repp J, Moresco F, Meyer G and Rieder K H 2000 *Phys. Rev. Lett.* **85** 2981
[68] Hyldgaard P and Persson M 2000 *J. Phys.: Condens. Matter* **12** L13
[69] Néel N, Kröger J and Berndt R 2005 *Adv. Mater.* at press
[70] Ortega J E, Mugarza A, Repain V, Rousset S, Pérez-Dieste V and Mascaraque A 2002 *Phys. Rev.* B **65** 165413
[71] Néel N, Kröger J and Berndt R 2005 *Appl. Phys. Lett.* submitted